GROWTH AND REABSORPTION IN BIOLOGICAL TISSUES

Joan O'Connor

Lavinia Maria Alves Borges

Fernando Pereira Duda

Antonio Guilherme Barbosa da Cruz

joan@mecsol.ufrj.br

lavinia@mecanica.coppe.ufrj.br

duda@mecanica.coppe.ufrj.br

aguicruz@mecanica.coppe.ufrj.br

Programa de Engenharia Mecnica/COPPE, Universidade Federal do Rio de Janeiro, Brazil

Abstract. *The development of computational tools to predict the long-term behavior of prosthetic devices in orthopedics may contribute to improve the quality of life of the elderly population, and has a tremendous importance since the proportion of this population is increasing. In this work, we investigate bone density growth for a healthy femur and a femur with prosthesis submitted to loads. We consider a growth and remodeling theories for biological materials and its treatment using continuum mechanics. Accordingly, kinematics, balance laws, constitutive equations, and governing equations resulting from the coupling of mass and momentum balances are presented. The biomechanical coupled problem obtained is approximated by a finite-element model and implemented using COMSOL Multiphysics. We present simulation examples for a healthy femur and a femur with prosthesis. For the first example, density growth is not consider, and daily activities load cases were take into account in order to locate possible growth or reabsorption zones. For the second example, density growth is simulated considering bone as homogeneous tissue. Numerical results show that the proposed approach has a great capability of predicting density profiles due to different types of loads and to locate bone growth or reabsorption zones for the situations of intact and prosthetic femur studied in this work.*

Keywords: *Bone tissue, Density growth, Continuum mechanics, Finite elements*

1 INTRODUCTION

Different diseases as osteoporosis among others, may lead to femoral bone fracture and the necessity of a surgical intervention to restore the articulation mobility with the use of prosthetic devices. This kind of surgical procedures are also carried out in order to eliminate pain and restore functionality in hips, due to other diseases such as osteoarthritis. This work deals with a finite element model for density growth process for a healthy femur and for a femur with a prosthesis, submitted to loads equivalent to daily activities loads, based on growth and remodeling theories for biological materials and its treatment using continuum mechanics (Cowin and Hegedus, 1975; Rodriguez et al., 1994; Kuhl and Steinmann, 2003a,b). Taking the multiplicative decomposition of the deformation gradient as starting point, there are defined the biological growth associated to soft tissues and the remodeling process associated to hard tissues, while the former is related with changes in volume at constant density, the latter is associated with changes in properties at constant volume (Taber, 1995). For density growth case, which is the focus of this work, the modeling approach of this biological process, is of a constitutive kind using continuum non linear mechanics for hard tissues (Kuhl and Steinmann, 2003a,b; Kuhl and Balle 2005).

The contribution of this work, is to implement the density growth process in a finite element model for a healthy femur and for a femur with prosthesis considering: The applied loads corresponding to real daily activities, and the complex geometry of whole femur from proximal to distal. In Section 2 we present the density growth theory within the context of the continuum mechanics including kinematics, balances laws for mass and linear momentum and constitutive equations, and the set of governing equations resulting from the coupling of biological and mechanical problems. Section 3 describes briefly how to solve the density evolution problem with COMSOL Multiphysics v 4.4 and the proposed model applications in two examples, a first one without consider density growth process for healthy and prosthetic femurs submitted to three daily activities time dependent loads to locate possible density growth zones, and a second one taking into account density growth process, considering bone as an homogeneous domain. Finally, results and discussions are presented in Section 4.

2 THEORETICAL FRAMEWORK

Let consider a body in the reference configuration $\mathcal{B}$ capable to change its density due to a mechanical stimulus. Two coupled processes are taking place in $\mathcal{B}$; a mechanical one, driven by the body deformation due to loads action and a biological one, related with density changes in an energy driven format due to a mass source. Body motion is given by the vector field χ, consequently, velocity field is $\mathbf{v} = \dot{\chi}$. Mapping $\mathbf{x} = \chi(\mathbf{X}, t)$ is considered one-to-one in $\mathbf{X}$ for fixed t, so invertible then: $\mathbf{X} = \chi^{-1}(\mathbf{x}, t)$, being $\mathbf{X}$ and $\mathbf{x}$, the position vectors referred to the reference and current configurations, respectively.

The deformation gradient is defined as $\mathbf{F} = \nabla\chi$ and the volumetric Jacobian of the deformation is the determinant of $\mathbf{F}$, being: $J = \det(\mathbf{F})$. Dot symbol and ∇ operator denote material time derivative and gradient of a quantity, respectively. The displacement $\mathbf{u}$ of $\mathbf{X}$ is defined as $\mathbf{u}(\mathbf{X}, t) = \chi(\mathbf{X}, t) - \mathbf{X}$, where its gradient is related with $\mathbf{F}$ through $\mathbf{F} = \mathbf{I} + \nabla\mathbf{u}$, where $\mathbf{I}$ is the second order identity tensor. Density growth process is regulated by the rate of the density scalar field ρ_K.

Bone only experiences infinitesimal strains within its physiological range, however, we adopted a non linear kinematic formulation for large deformations, following Pang et al. (2012). Balance laws and constitutive theory to solve the density growth problem are presented following Kuhl and Steinmann (2003b).

2.1 Balance equations

Mass and momentum balances are presented in the local form referred to the reference configuration. The rate change of mass due to volumetric mass sources, neglecting mass fluxes, is:

$$\dot{\rho}_K = \Gamma_K \tag{1}$$

expressing the equilibrium of the rate change of mass $\dot{\rho}_K$ with the mass source Γ_K, where ρ_K is the mass density in the reference configuration and Γ_K is the mass source.

The linear momentum balance, balances the rate change of momentum density $\dot{\overline{\rho_K \mathbf{v}}}$ with the momentum contributions of traction, body forces and mass source as:

$$\dot{\overline{\rho_K \mathbf{v}}} = \mathrm{Div}\mathbf{P} + \mathbf{b} + \Gamma_K \mathbf{v} \tag{2}$$

being $\mathbf{v}$ the velocity, $\mathbf{b}$ the body force and $\mathbf{P}$ the first Piola-Kirchhoff stress tensor. Div denotes the divergence of a quantity. Considering (1) in (2), the linear momentum balance gives:

$$\rho_K \dot{\mathbf{v}} = \mathrm{Div}\mathbf{P} + \mathbf{b} \tag{3}$$

2.2 Constitutive equations

Adopting the multiplicative decomposition of the deformation gradient (Rodriguez et al., 1994) as $\mathbf{F} = \mathbf{F}_g \mathbf{F}_e$, and assuming that density growth in hard tissues occurs at constant volume, intermediate configuration is not necessary, then: $\mathbf{F}_g = 1$ and $\mathbf{F} = \mathbf{F}_e$, where $\mathbf{F}_g$ is the growth deformation gradient and $\mathbf{F}_e$ is the elastic deformation gradient.

In the mass balance of (1), the mass source term Γ_K has the following form (Harrigan and Hamilton, 1993):

$$\Gamma_K = c\left(\left[\frac{\rho_K}{{\rho_K}^*}\right]^{-m} \psi_K - {\psi_K}^*\right) \tag{4}$$

being ${\rho_K}^*$ the initial density in the reference configuration, ${\psi_K}^*$ the initial free energy or stimulus atractor (Carter and Beaupre, 2007), m the exponent needed for bone adaptation process (Harrigan and Hamilton, 1993), and c the coefficient that governs the speed of adaptation process (Kuhl and Steinmann, 2003b). The free energy form adopted is:

$$\psi_K = \left[\frac{\rho_K}{{\rho_K}^*}\right]^n {\psi_K}^{neo} \tag{5}$$

with the relative density term $[\rho_K/{\rho_K}^*]^n$ used for open pored cell materials (Carter and Hayes, 1977; Gibson and Ashby, 1982), where the porosity exponent n varies from 1 to 3.5. An additional assumption is neglect tissues viscous effects for short time scales and consider the constitutive response as hyperelastic (Kuhl and Balle, 2005), consequently, free energy function considered is of a Neo-Hookean hyperelastic type for isotropic materials:

$$\psi_K{}^{neo} = \left[\frac{\lambda}{2}\ln^2 J + \frac{\mu}{2}\left(\mathbf{F}^T\mathbf{F} : \mathbf{I} - 3 - 2\ln J\right)\right] \tag{6}$$

where λ and μ are the Lame constants.

Piola-Kirchoff Stress can be obtained through the free energy derivative with respect to the deformation gradient, hence, using (5) and (6):

$$\mathbf{P} = \frac{\partial \psi_K}{\partial \mathbf{F}} = \left[\frac{\rho_K}{\rho_K{}^*}\right]^n \left[(\lambda \ln J - \mu)\mathbf{F}^{-T} + \mu \mathbf{F}\right] \tag{7}$$

2.3 Governing equations and boundary conditions

The governing equations are obtained coupling the biological problem, defined through the mass balance, with the mechanical problem defined through the momentum balance. The biological problem expression is obtained using the free energy of (5) for an hyperelastic material in the form of (6), and the mass source (4) in the mass balance (1). The mechanical problem expression is obtained using the Piola-Kirchoff stress of (7) in the momentum balance (3), resulting in:

$$\dot{\rho}_K = \frac{1}{2}\left[\frac{\rho_K}{\rho_K{}^*}\right]^{n-m} \left[\lambda \ln^2(J) + \mu\left[\mathbf{F}^T\mathbf{F} : \mathbf{I} - 3 - 2\ln(J)\right]\right] - \psi_K^* \tag{8}$$

$$\mathbf{0} = \mathrm{Div}\left(\left[\frac{\rho_K}{\rho_K{}^*}\right]^n \left[(\lambda \ln J - \mu)\mathbf{F}^{-T} + \mu \mathbf{F}\right]\right) \tag{9}$$

considering a quasi-static process and neglecting body forces.

The boundary conditions that supplement the above governing equations can be established as follows: Let the body $\mathcal{B}$ be given with loading surface tractions $\bar{\tau}$ defined on $\partial_\tau \mathcal{B}$, and with prescribed displacements $\bar{\mathbf{u}} = 0$ on $\partial_u \mathcal{B}$, then, Neumann and Dirichlet Boundary Conditions (BC) for the mechanical problem are, respectively

$$\begin{aligned} \mathbf{P}(\mathbf{X})\mathbf{n}(\mathbf{X}) &= \bar{\tau}(\mathbf{X}), \qquad && \mathbf{X} \in \partial_\tau \mathcal{B} \\ \mathbf{u}(\mathbf{X}) &= \bar{\mathbf{u}}(\mathbf{X}), \qquad && \mathbf{X} \in \partial_u \mathcal{B} \end{aligned} \tag{10}$$

where $\mathbf{n}$ is the unit normal to $\partial_\tau \mathcal{B}$. Prescribed displacements $\bar{\mathbf{u}}$ and prescribed tractions $\bar{\tau}$ are given functions on $\partial_u \mathcal{B}$ and $\partial_\tau \mathcal{B}$ which are respectively, complementary disjoints of $\partial \mathcal{B}$. Within the mechanical problem is embedded the biological density growth boundary value problem given by the mass balance (1), with the initial condition:

$$\rho_K(\mathbf{X}, 0) = \rho_K{}^* \tag{11}$$

3 NUMERICAL APPLICATION

To solve the theoretical model presented, we have used COMSOL Multiphysics v 4.4. The goal is to solve the incremental problem of density evolution due to the mass source Γ_K for an hyperelastic material, embedded into the mechanical problem, which is coupled to density through the deformation field generated in response to the applied load. The free energy function was reprogrammed including the relative density term in the Neo-Hookean hyperelastic free energy. A function for the mass source term Γ_K was also implemented in the form of (4). In this section are presented three application examples. All models were discretized with Lagrangian quadratic elements to interpolates displacements $\mathbf{u}$ and the density ρ_K. For the time discretization, a General-α backward differentiation method was used. We have used the MUMPS solver to solve the discrete system resulting from each time step discretization with a residual tolerance levels of 10^{-4}, which is considered to be sufficient since similar solutions were obtained at lower tolerance levels. In all models, plane stress condition was adopted.

3.1 Geometrical model

The geometrical two-dimensional (2D) model for healthy femur and for femur with prosthesis is shown in Fig. 1, and corresponds to a 2D slice through the whole femur in the mid-frontal plane, for both cases: for a healthy femur (HF) and for a femur with prosthesis (FP). Cortical and spongious tissues contours were obtained in previous works (O'Connor et al., 2011) and were compared with femur anatomical standard dimensions (Husmann et al., 1997).

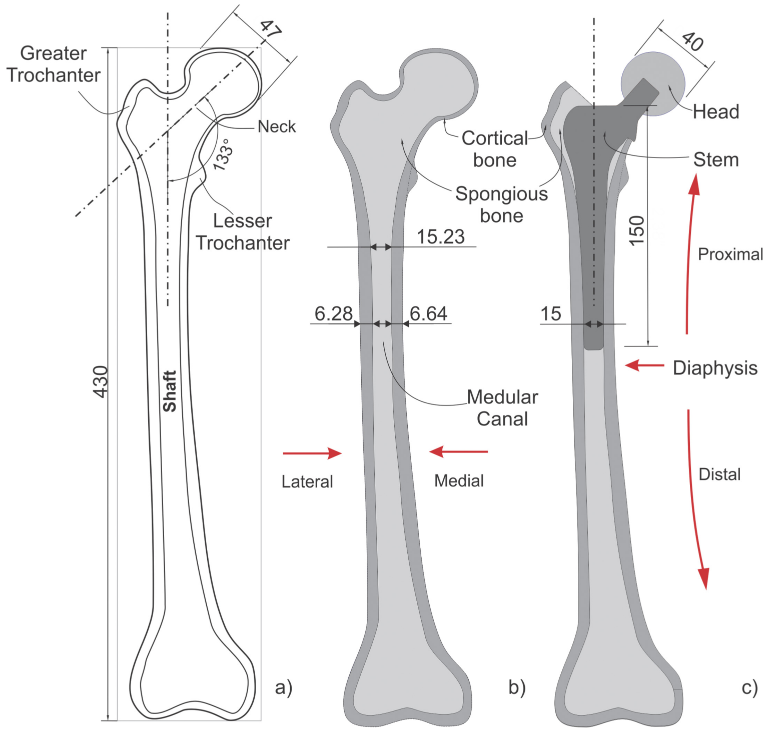

Figure 1: Healthy femur (HF) and the femur with prosthesis (FP). a), b) Healthy femur: total length, neck-shaft angle ($133°$), femoral head diameter, medular canal diameter and cortical wall thickness near the middle diaphysis by medial and lateral. c) Femur with prosthesis: prosthesis stem length 150 mm and size 15 mm (diameter), head diameter 40 mm. *All dimensions are in millimeters

Tissue contours Splines and its resultants closed spaces were converted to 2D surfaces to generate cortical and spongious domains. Prosthesis is considered as conceptual, with typical dimensions from specialized literature (Sastre et al., 2004), and its geometrical domains were obtained using CAD tools. The final model coupled structure-structure was build using boolean operations.

3.2 Example 1: Dynamic model without consider density growth

It was implemented a FE model, without consider density growth, for a HF and for a FP, submitted to three daily activities loads: normal walk, going up stairs and going down stairs, to locate high stress points (Fig. 2). Zero displacements Dirichlet BC were assumed in femurs distal ends (Fig. 2 a.1). Load functions (Fig. 2 a.2) were taken from public database Orthoload (Bergmann, 2009), and were applied in the femoral and prosthesis heads in -y direction as distributed loads (Fig. 2 a).

Cortical and spongious tissues were considered as hyperelastic materials with Lame constants $\lambda_c = 9230$ MPa and $\mu_c = 6153$ MPa, for cortical and $\lambda_s = 1153$ MPa and $\mu_s = 769$ MPa for spongious bones, Kuhl and Balle (2005). Prosthesis materials considered were: Titanium Ti6Al4V alloy for the stem, with Young's modulus $E = 110000$ MPa and Poisson $\nu = 0.3$, and 316L surgical steel for the head with $E = 230000$ MPa and $\nu = 0.3$, considered as linear elastics (Sastre et al., 2004). The model was discretized in 27712 elements (Fig. 2 b), and solved for 118914 degrees of freedom (DOF). The time interval for the simulations was $t = 1.49s$ corresponding to 100% of one entire cycle for each load case, and time step used was $\Delta t = 0.01$.

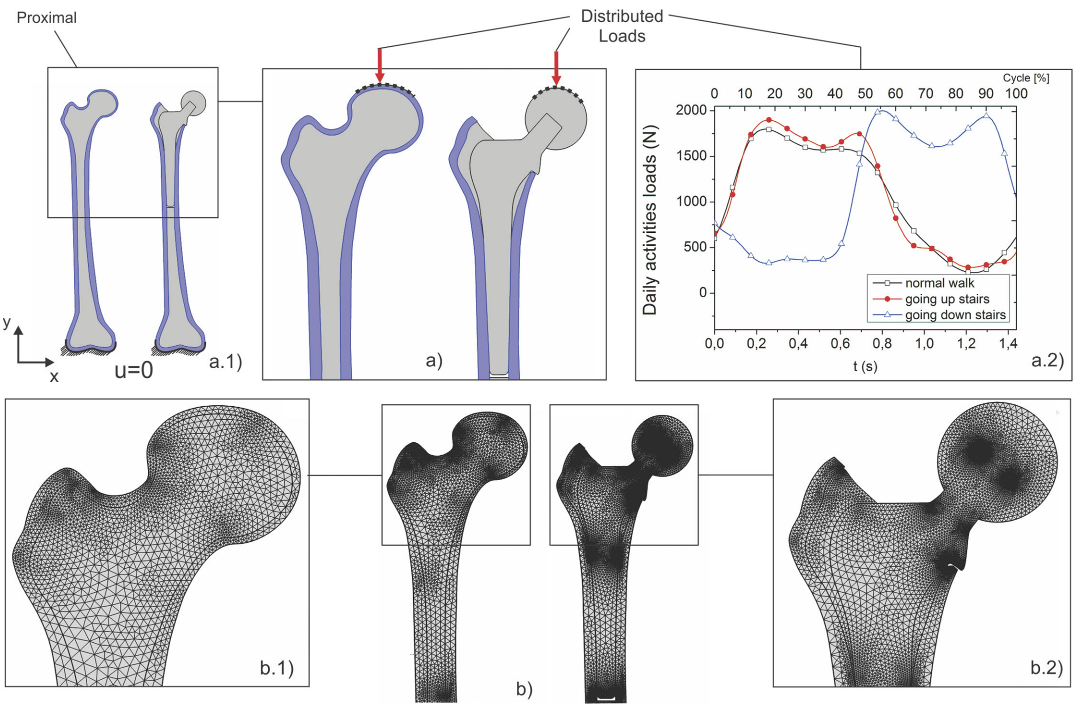

Figure 2: Boundary conditions, loads and mesh for the HF and for the FP. a) Proximal part of the model domains and applied load regions. a.1) Dirichlet boundary conditions a.2) Daily activities loads values over time for a 100% of one cycle *taken from public data base Orthoload (Bergmann, 2009). b) Mesh of the proximal part of HF and FP. b.1), b.2) Meshes zoom.

Results analysis

Stress results were analyzed and there were found three main critical points, coincident in location for the three load cases. Region 1: located in the medial cortical wall HF diaphysis, region 2: in medial cortical wall FP diaphysis, and region 3: at the inferior HF neck (Fig. 3 a).

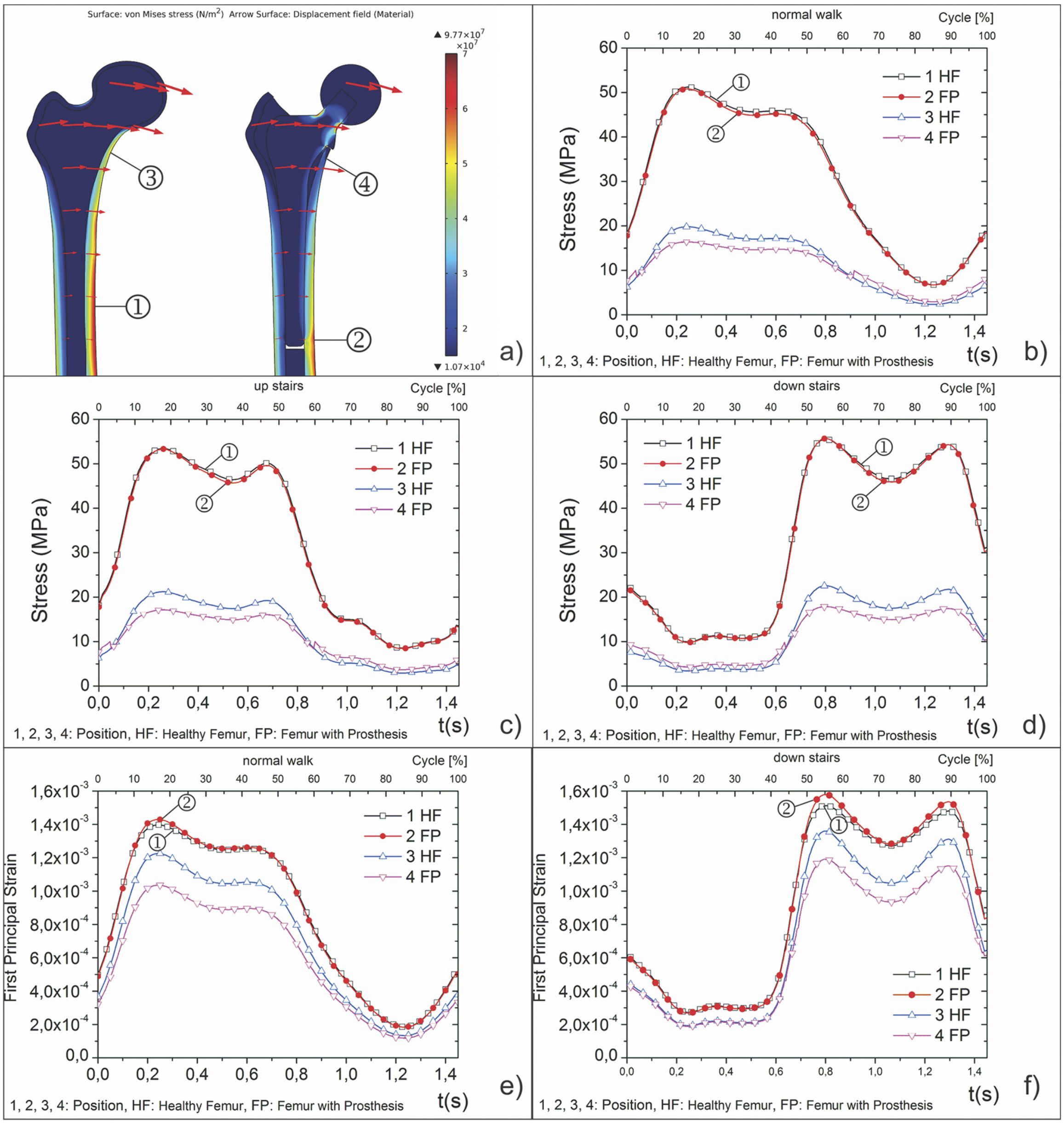

Figure 3: Von Mises stress results and critical points for load cases simulated. a) Von Misses stress distribution for the normal walk peak load at $t = 0.245$ s, red arrows describes the displacements vector field. Von Mises stress vs. time values measured in regions 1, 2, 3 and 4 for: b) Normal walk. c) Up stairs. d) Down stairs. Strains vs. time values measured in regions 1, 2, 3 and 4 for: e) Normal walk. f) Down stairs.

A region 4, located at the inferior FP neck, was added to the analysis to compare the critical regions for both situations, healthy femur and with prosthesis. Figure 3 b, c, d show the Von Mises stress vs time in the regions of interest for the three load cases, showing that stress values in zones 1 and 2 were slightly similar and were higher for going down stairs case.

In region 3, stresses were higher than in region 4 for the three load cases, this difference is a result of an unloaded situation in the FP proximal part. Strains for normal walk and going down stairs are shown in Fig. 3 e, f, where the values for regions 1 and 2 were similar and there was found a difference again between 3 and 4, meaning that mobility in FP is lower than in HF. Results were compared with other authors works (Wagner et al., 2010) showing agreement. Stresses corresponds to current configuration in which Cauchy and Piola-Kirchoff stresses are related through $\mathbf{P} = J\mathbf{T}\mathbf{F}^{-T}$, where $\mathbf{T}$ is the Cauchy stress and $\mathbf{F}^{-T}$ denotes the inverse of the transpose of $\mathbf{F}$. Von Mises stress for the regions of interest were below of cortical bone compressive and tensile yield strength values σ_{yc} = 182 MPa and σ_{yt} = 115 MPa (Cowin and Doty, 2007), without compromise bone integrity. In the prosthesis, higher stresses were found between 70 to 97 MPa in the inferior and superior necks, showing agreement with Bougherara et al. (2010), this values were below the compressive and tensile yield strength for titanium alloy Ti6Al4V of σ_{yc} = 970 MPa and σ_{yt} = 880 MPa.

3.3 Example 2: Density growth for homogeneous bone

Density growth is implemented following formulation presented in sections 2 and 3. It was used the previous example geometry without consider the spongious bone, hence, bone was treated as homogeneous. A multiple step load was used from 0 N to 1850 N for 7 time steps with increments of 250 N constant values on each unit time step, the first time step was divided in two sub-steps, a ramp 100 N load from $t = 0$ to $t = 0.1$ followed by a 250 N constant value from $t = 0.1$ to $t = 1$. Load values considered are in correspondence with daily activities loads analyzed in example 1, and were applied in the femur and prosthesis heads in the *-y* direction. Zero displacements BC were considered in femurs distal ends. The multiple step load form was chosen assuming that total time for daily load cases corresponding to one cycle is too small and load values are too high for density growth process takes place, therefore, we use a multiple step load following Kuhl and Steinmann (2003b). Lame constants were $\lambda_c = 9230$ MPa and $\mu_c = 6153$ MPa for homogeneous bone, considered as hyperelastic material. Properties of example 1 were considered for prosthesis components. Initial density was $\rho_K{}^*$ = 800 $\mathrm{kg/m^3}$, the attractor was $\psi_K{}^* = 0.01$ MPa according to Kuhl and Steinmann (2003b) and (Carter and Beaupre, 2007), as well as values of $n = 2$ and $m = 3$. Simulation time interval was $t = 7$ dimensionless time units, and time step for the incremental problem was $\Delta t = 0.05$. The model was discretized in 28940 elements and solved for 153805 DOF.

Results for homogeneous bone model

Density distribution at: $t = 4.5$, $t = 5.5$ and $t = 7$ is shown in Fig. 4 a, b, c. Results are in agree with real bone density values. Cortical walls, of around 1800 $\mathrm{kg/m^3}$ were formed in medial and lateral parts (in red) and spongious bone areas with values of around 800 $\mathrm{kg/m^3}$ were formed in the medular canal (in blue) for HF and FP (Fig. 4 c). Proximal femur density distribution (HF in Fig. 4 c) also agrees with the trabecular bone arrange and cortical walls of an anatomical femur (Kuhl and Steinmann, 2003a, b). Ward's triangle, spongious column from the head to the inferior neck, and the system formed from the lateral cortical bone to the superior neck, were well reproduced in the density distribution (Fig. 4 c). Density evolution in the zones of interest was measured over time (Fig. 4 e), showing the problem non linearity associated to the coupling, and the time dependent nature of the mass balance.

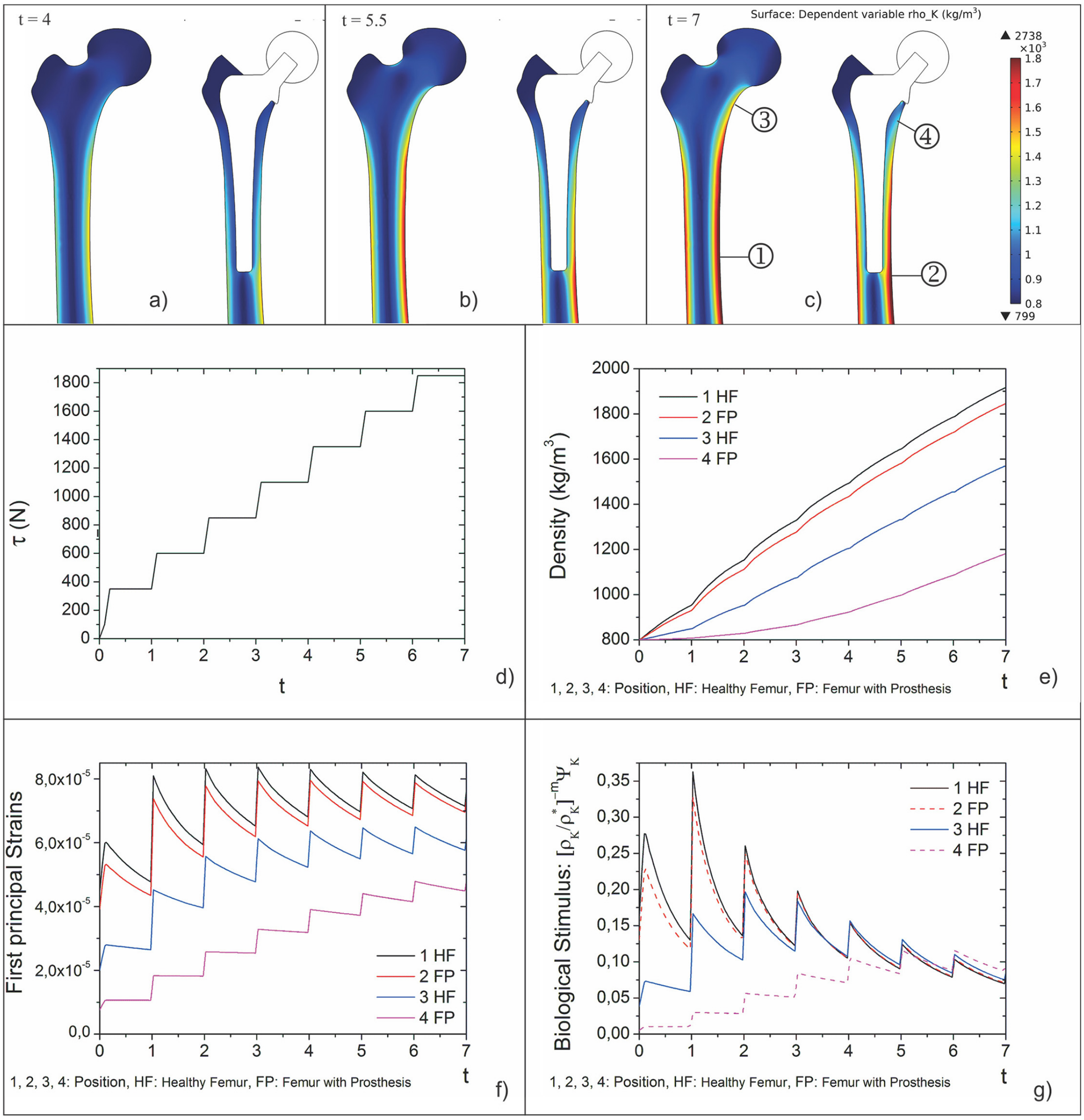

Figure 4: Density prediction for the healthy femur and for the femur with prosthesis; loads, density evolution, strains and biological stimulus in the regions of interest. a-c) Density prediction for HF and for FP at times: $t = 4.5$, $t = 5.5$ and $t = 7$, where 1, 2, 3 and 4 are the regions of interest d) Multiple step load e) Density evolution f) Strains g) Biological stimulus

Density exhibits a relaxation tendency to biological equilibrium (Fig. 4 e) and higher values were found, in zones 1 and 2. The maximum in zone 1 of 1915 $\mathrm{kg/m^3}$ was slightly greater than cortical bone density, however, the rest of the zones in medial and lateral cortical walls were in agreement with cortical bone density (Fig. 4 e). In 4, lower densities were found around 1000 $\mathrm{kg/m^3}$ in contrast with the 1550 $\mathrm{kg/m^3}$ found in the same region of HF, this lower values (as a result of the unload situation in the proximal part, because the stresses are transmitted to prosthesis distal ends), could cause bone reabsorption and may lead, eventually, to the prosthesis aseptic loosening.

In Fig. 4 f, g, are shown the strains and biological stimulus, showing the non linear behaviour and quantities relaxation towards to biological equilibrium. In agreement with Kuhl and Steinmann (2003b), each increase of loading $\bar{\tau}$ is followed by changes in density and strains converging to a new equilibrium state, where the biological stimulus equals the stimulus attractor ${\psi_K}^*$, the mass source Γ_K vanishes and ρ_K undergo no further changes, providing to HF and to FP the optimal density distribution to support loads considered.

4 DISCUSSION

A density growth model for hard tissues was presented in this work based on growth and remodeling theories, and was implemented in a finite element software to simulates the behavior of a healthy femur and a femur with a prosthesis submitted to loads. Regarding to model limitations we can cite, its bi-dimensional nature and the effect of neglect abductors muscle forces, so the extension to tridimensional model and the inclusion of muscle forces in the analysis, together with a comparison with clinical cases and consider a failure criteria taking into account porosity, are among the aspects to include for future works. However, the model presented, reproduces optimally the biological forms and the tissue-implant interfaces, and as a consequence, the model can capture the physics of the problem accurately. The model consider not only the proximal but also the distal part of the femur. This fact represents a more accurately model, since boundary condition are more realistic than the boundary conditions adopted by other authors considering only the proximal part. Predicted density distribution agrees with real bone density distributions reported in literature, for the model presented. This density distribution results can be used, in combination with the dynamic model presented (which takes into account different daily activities loads) as a predictive medical tool to locate zones of density growth or reabsorption under different loads situations for an intact femur and for a femur with prosthesis.

Important results were obtained from the comparison of zones 3 and 4, as the identification of lower density zones in the femur with prosthesis due to the unloaded situation in the proximal part, that may lead to bone reabsorption with the consequent aseptic loosening of the implant. Another important result is the hypothesis that for the daily activities loads, in the prosthesis case, an increase of load is needed to reach the bone density values corresponding to the healthy condition. As a proposal, it is suggested to evaluate this situation by clinicians, and possibly to modify fisio-therapeutic plans for hip prosthesis patients, in order to reach adequate density values during clinical recovery phase after surgery. In summary, the proposed density growth models in conjunction with the dynamical model for daily activities loads, represents a potential powerful tool for medical applications, specifically, in hip prosthesis and degenerative bone diseases research areas, to predict density profiles due to different loads regimes and to detect zones of bone density growth and bone reabsorption, for intact femur and for femur with prosthesis.

ACKNOWLEDGEMENTS

The authors gratefully acknowledge the financial support provided by CNPQ under grant (870068/1997.0) and CAPES PROEX (31001017030D4)

REFERENCES

Bergmann., G., 2009. *Orthoload. (ed.),*. Charite Universitaetsmedizin Berlin (2008). Retrieved Feb. 1, 2009 (from http://www.OrthoLoad.com).

Bougherara, H., & Zdero, R., & Shah, S., & Miric, M., & Papini, M., & Zalzal, P., & Schemitsch, E. H., 2010. A biomechanical assessment of modular and monoblock revision hip implants using FE analysis and strain gage measurements. *Journal of orthopaedic surgery and research*, vol. 5, n. 1, pp. 34.

Carter, D. R., & S Beaupré, G. S., 2007. *Skeletal Function and Form: Mechanobiology of Skeletal Development, Aging, and Regeneration*. Cambridge University Press.

Carter, D. R., & Hayes, W. C., 1977. The compressive behavior of bone as a two-phase porous structure. *The Journal of Bone & Joint Surgery*, vol. 59, n. 7, pp. 954-962.

COMSOL, 2013. *COMSOL Multiphysics. Reference Manual.* 2013 version 4.4

Cowin, S. C., & Doty, S. B., 2007. *Tissue Mechanics*. Springer.

Cowin, S. C., & Hegedus, D. H., 1976. Bone remodeling I: theory of adaptive elasticity. *Journal of Elasticity*, vol. 6, n. 3, pp. 313-326.

Doblaré, M., & García, J. M., & Gómez, M. J., 2004. Modelling bone tissue fracture and healing: a review. *Engineering Fracture Mechanics*, vol. 71, n. 1314, pp. 1809-1840.

Gibson, L. J., & Ashby, M. F., 1982. The mechanics of three-dimensional cellular materials. *Proceedings of the Royal Society of London. A. Mathematical and Physical Sciences*, vol. 382, pp. 43-59.

Harrigan, T. P. & Hamilton, J. J., 1993. Finite element simulation of adaptive bone remodelling: a stability criterion and a time stepping method. *International Journal for Numerical Methods in Engineering*, vol. 36, n. 5, pp. 837-854.

Husmann, O., & Rubin, P. J., & Leyvraz, P., & de Roguin, B. & Argenson, J., 1997. Three-dimensional morphology of the proximal femur. *The Journal of Arthroplasty*, vol. 12, n. 4, pp. 444-450.

Kuhl, E., & Balle, F., 2005. Computational modeling of hip replacement surgery: Total hip replacement vs. hip resurfacing. *Technische mechanik*, vol. 25, n. 2, pp. 107-114.

Kuhl, E., & Steinmann, P., 2003a. Mass and volume specific views on thermodynamics for open systems. *Proceedings of the Royal Society of London. Series A Mathematical, Physical and Engineering Sciences*, vol. 459, n. 2038, pp. 2547-2568.

Kuhl, E., & Steinmann, P., 2003b. Theory and numerics of geometrically non-linear open system mechanics. *International Journal for Numerical Methods in Engineering*, vol. 58, n. 11, pp. 1593-1615.

O'Connor, J., & Rodriguez, M., & Calas, H., & Moreno, E., & Palomares, E., 2011. Modelación y simulación de sistemas biomecánicos acoplados utilizando el método de elementos finitos. Aplicaciones en ortopedia. *IFMBE Proceedings: V Latin American Congress on Biomedical Engineering CLAIB 2011*, vol. 33, pp. 619-622.

Pang, H., & Shiwalkar, A. P., & Madormo C. & Taylor R. E. & Andriacchi T. P. & Kuhl E., 2012. Computational modeling of bone density profiles in response to gait: a subject-specific approach. *Biomechanics and Modeling in Mechanobiology*, vol. 11, n. 3-4, pp. 379-390.

Rodriguez, E., & Hoger, A., & McCulloch, D., 1994. Stress dependent finite growth in soft elastic tissues. *Journal of Biomechanics*, vol. 27, n. 4, pp. 445-467.

Sastre, R., & Aza, S., & San Roman, J., 2004. *Biomateriales*. Faenza Editrice Ibrica.

Taber, L. A., 1995. Biomechanics of growth, remodeling, and morphogenesis. *Applied Mechanics Reviews*, vol. 48, n. 8, pp. 487-545.

Wagner, D. W., & Divringi, K., & Ozcan, C., & Grujicic, M., & Pandurangan, B., & Grujicic, A., 2010. Combined musculoskeletal dynamics structural finite element analysis of femur physiological loads during walking. *Multidiscipline Modeling in Materials and Structures*, vol. 6, n. 4, pp. 417-437.